

# Magnetic properties and large magneto-caloric effect in the amorphous $\text{Ho}_{0.2}\text{Tm}_{0.2}\text{Gd}_{0.2}\text{Co}_{0.2}\text{Al}_{0.2}$ ribbon

Yongyun Shu<sup>a</sup>, Longfei Wang<sup>b</sup>, Silu Huang<sup>a</sup>, Yikun Zhang<sup>a,b,\*</sup>

<sup>a</sup> School of Electronics and Information, Hangzhou Dianzi University, Hangzhou 310018, China

<sup>b</sup> Key Laboratory of Novel Materials for Sensor of Zhejiang Province, Hangzhou Dianzi University, Hangzhou 310012, China

## ARTICLE INFO

### Keywords:

Magneto-caloric (MC) effect  
Amorphous  $\text{Ho}_{0.2}\text{Tm}_{0.2}\text{Gd}_{0.2}\text{Co}_{0.2}\text{Al}_{0.2}$  ribbon  
Rare earth  
Magnetic properties

## ABSTRACT

We fabricated the amorphous  $\text{Ho}_{0.2}\text{Tm}_{0.2}\text{Gd}_{0.2}\text{Co}_{0.2}\text{Al}_{0.2}$  ribbon by melt-spun method and systematically investigated its glass forming ability (GFA) and magnetic properties, especially of the magnetic phase transition (MPT) and magneto-caloric (MC) effect. The melt-spun  $\text{Ho}_{0.2}\text{Tm}_{0.2}\text{Gd}_{0.2}\text{Co}_{0.2}\text{Al}_{0.2}$  ribbon is found to exhibit a fully amorphous structure and good GFA. The amorphous  $\text{Ho}_{0.2}\text{Tm}_{0.2}\text{Gd}_{0.2}\text{Co}_{0.2}\text{Al}_{0.2}$  ribbon undergoes a second order type MPT around 32.6 K from ferromagnetic to paramagnetic state. Large reversible low temperature MC effect and good MC performances in the amorphous  $\text{Ho}_{0.2}\text{Tm}_{0.2}\text{Gd}_{0.2}\text{Co}_{0.2}\text{Al}_{0.2}$  ribbon were realized which was identified by the parameters of magnetic entropy change, temperature-averaged entropy change, and refrigerant capacity. These parameters are at similarly high level with recently reported low temperature MC materials, making the amorphous  $\text{Ho}_{0.2}\text{Tm}_{0.2}\text{Gd}_{0.2}\text{Co}_{0.2}\text{Al}_{0.2}$  ribbon also attractive for magnetic cooling.

## 1. Introduction

The development of magnetic functional materials has always been at the forefront of materials science and technology due to their interesting magneto-properties and potential applications [1–8] in many advanced industry fields. The solid-state magnetic cooling [1–4] which is based on magneto-caloric (MC) effects of magnetic solids has received much research interests due to its remarkable benefits in both social and economic aspects. The MC effect is a magneto-thermodynamic property [1–4] which can be manipulated by the changes of temperature (adiabatic process) or magnetic part of entropy (isothermal process) by the change of external magnetic field. Thus, many rare earths (RE)-based and/or transition metal (TM)-based magnetic solids [1–4,9–18] have been determined with respect to their MC effects over the last several decades and some of them have been reported to exhibit large MC effects and good MC performances, such as, the  $\text{La}(\text{Fe},\text{Si})_{13}\text{H}_y$ ,  $\text{RE}(\text{Al},\text{Co},\text{Ni})_2$ ,  $\text{RE}_2\text{TM}'\text{TM}''\text{O}_6$ ,  $\text{Mn-Fe-P-X}$ ,  $\text{Mn}_{30}(\text{Fe},\text{Cu})_{20}\text{Al}_{50}$ ,  $\text{Ni-Mn-X}$ , etc. However, large gaps are still existed in the MC performances between the requirement of magnetic cooling and reported magnetic solids. Thus, developing suitable magnetic solids with large MC effects and good MC performances remains the urgent task for practical magnetic cooling.

Among the reported magnetic solids with good MC performances, the RE-TM-based alloys and oxides [19–29] are of great interests for the

low temperature magnetic cooling. For examples, we have recently reported low temperature giant MC effects in the antiferromagnetic (AFM)  $\text{Gd}_2\text{MgTiO}_6$  oxide [21] and  $\text{GdFe}_2\text{Si}_2$  compound [22] which were related to their own unique unstable ground state. Large low  $\Delta H$  induced low temperature MC effects have also been very recently reported in the  $\text{Er}_{1-x}\text{Tm}_x\text{Al}_2$ ,  $\text{LiErF}_4$  and  $\text{GdMo}_{0.5}\text{Ti}_{0.5}\text{O}_4$ , and  $\text{GdCoC}$  compounds [25–28]. The magnetic and MC properties in the  $\text{RE}_2\text{BaZnO}_5$  oxides [29] were investigated by Xu *et al.*, in which large low temperature MC effects have been realized below 5 K with the maximum magnetic entropy change ( $-\Delta S_M^{\text{max}}$ ) values range from 16.9 to 10.3 J/kgK under the magnetic field change  $\Delta H = 0-5$  T.

Moreover, the MC effects in some amorphous RE-TM-based alloys [30–35] have recently received increasing research interests. For examples, the glassy formation ability (GFA) and MC effects of binary amorphous Tb–Ni alloys [30] were determined by Pan *et al.*, in which the amorphous  $\text{Tb}_{65}\text{Ni}_{35}$  alloy exhibits good GFA and large MC effect around 64 K with the  $-\Delta S_M^{\text{max}}$  of 8.7 J/kgK under  $\Delta H = 0-5$  T [30]. The MC effects and critical behavior in the amorphous  $\text{Eu}_{80}\text{Au}_{20}$  alloy [31] were investigated by Lassri *et al.*, in which a large relative cooling power (RCP) was reported. The magnetic and MC properties in the ternary amorphous  $\text{RE}_{55}\text{Co}_{17.5}\text{Al}_{27.5}$  alloys [32] were determined by Jin *et al.*, these amorphous alloys are found to be good candidate materials for hydrogen liquefactions. The ternary amorphous Tm–Cu–Al alloys [33]

\* Corresponding author at: School of Electronics and Information, Hangzhou Dianzi University, Hangzhou 310018, China.

E-mail address: [ykzhang@hdu.edu.cn](mailto:ykzhang@hdu.edu.cn) (Y. Zhang).

<https://doi.org/10.1016/j.jnoncrysol.2024.122846>

Received 13 November 2023; Received in revised form 7 January 2024; Accepted 19 January 2024

Available online 28 January 2024

0022-3093/© 2024 Elsevier B.V. All rights reserved.

with good low temperature MC performances were designed by Ma *et al.*, in which the amorphous  $(\text{TM}_{67}\text{Cu}_{33})_{80}\text{Al}_{20}$  alloy [33] exhibits large MC effect around 4.5 K with the  $-\Delta S_{\text{M}}^{\text{max}}$  of 13.4 J/kgK under  $\Delta H = 0-5$  T. Very recently, good GFA and large low temperature MC effects in the quaternary  $\text{RE}_{55}\text{Co}_{30}\text{Al}_{10}\text{Si}_5$  amorphous alloys [34] was realized by Tian *et al.*, which could be good candidate materials for hydrogen liquefaction. The quinary amorphous Gd-Fe-Co-Al-Si alloys [35] were fabricated by Lindner *et al.*, in which tunable low temperature MC effects were realized. These studies indicated that there are some RE-TM-based amorphous alloys are with high potentials to possess good low temperature MC performances, which are deserved to be further determined.

In continuation of our series work on the investigation of magnetic and MC properties of the RE-TM-based magnetic solids [18–22], herein, we fabricated the amorphous  $\text{Ho}_{0.2}\text{Tm}_{0.2}\text{Gd}_{0.2}\text{Co}_{0.2}\text{Al}_{0.2}$  ribbon by melt-spun method and systematically investigated its structure, GFA, MPT and MC effect. Large reversible low temperature MC effects and good MC performances around 32.6 K were realized, making it attractive for practical low temperature magnetic cooling.

## 2. Experimental detail

The amorphous  $\text{Ho}_{0.2}\text{Tm}_{0.2}\text{Gd}_{0.2}\text{Co}_{0.2}\text{Al}_{0.2}$  ribbon was fabricated by two steps. Firstly, the ingot of  $\text{Ho}_{0.2}\text{Tm}_{0.2}\text{Gd}_{0.2}\text{Co}_{0.2}\text{Al}_{0.2}$  alloy was fabricated by conventional arc-melting technology from Ho (99.9 %), Tm (99.9 %), Gd (99.8 %), Co (99.95 %), and Al (99.8 %) metals with high purity under the Argon atmosphere. The alloy ingot was flipped over after each melting and re-melted three times to ensure homogeneity. Then, the amorphous  $\text{Ho}_{0.2}\text{Tm}_{0.2}\text{Gd}_{0.2}\text{Co}_{0.2}\text{Al}_{0.2}$  ribbon was obtained by melt-spun the ingot on a Cu-wheel (surface speed  $\sim 35$  m/s) with a water-cycle cooling system. The amorphous nature and GFA of  $\text{Ho}_{0.2}\text{Tm}_{0.2}\text{Gd}_{0.2}\text{Co}_{0.2}\text{Al}_{0.2}$  ribbon were checked by the X-ray diffraction (XRD, Rigaku SmartLab-9kW) and differential scanning calorimeter (DSC, Netzsche STA-449) technology. The magnetization data of the amorphous  $\text{Ho}_{0.2}\text{Tm}_{0.2}\text{Gd}_{0.2}\text{Co}_{0.2}\text{Al}_{0.2}$  ribbon was obtained by the magnetic properties measurement system (MPMSQ3, QD).

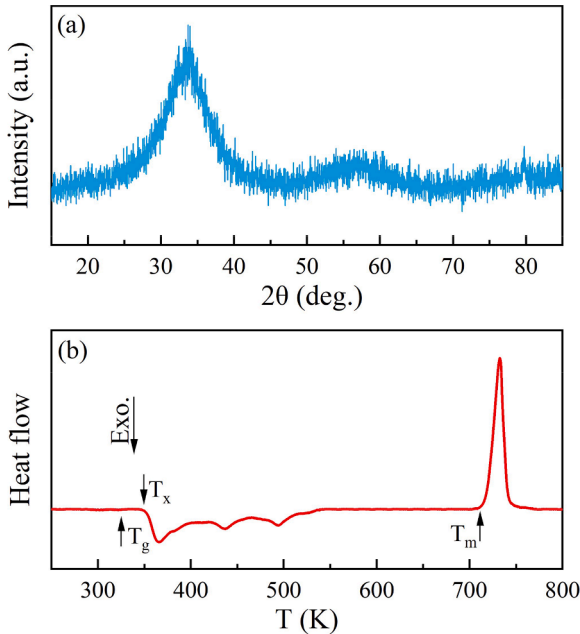


**Fig. 1.** (a) XRD patterns of the amorphous  $\text{Ho}_{0.2}\text{Tm}_{0.2}\text{Gd}_{0.2}\text{Co}_{0.2}\text{Al}_{0.2}$  ribbon. (b) DSC traces of the amorphous  $\text{Ho}_{0.2}\text{Tm}_{0.2}\text{Gd}_{0.2}\text{Co}_{0.2}\text{Al}_{0.2}$  ribbon.

## 3. Results and discussion

The room temperature XRD pattern of the amorphous  $\text{Ho}_{0.2}\text{Tm}_{0.2}\text{Gd}_{0.2}\text{Co}_{0.2}\text{Al}_{0.2}$  ribbon is given in Fig. 1(a). No observable Bragg diffraction peak in the patterns can be noted. Only two distinct broad humps which is typical fully amorphous structure behavior, illustrating fully amorphous state nature for present studied  $\text{Ho}_{0.2}\text{Tm}_{0.2}\text{Gd}_{0.2}\text{Co}_{0.2}\text{Al}_{0.2}$  ribbon. Additionally, the DSC trace of the amorphous  $\text{Ho}_{0.2}\text{Tm}_{0.2}\text{Gd}_{0.2}\text{Co}_{0.2}\text{Al}_{0.2}$  ribbon was also determined to further evaluate its GFA, and the results are given in Fig. 1(b). Apparently, a small endothermic reaction peak at lower temperature can be observed which is related to the glassy transition (named as the temperature of glassy transition,  $T_g$ ), suggesting the initial formation of the amorphous structure nature for present melt-spun  $\text{Ho}_{0.2}\text{Tm}_{0.2}\text{Gd}_{0.2}\text{Co}_{0.2}\text{Al}_{0.2}$  ribbon. Moreover, three significant exothermic peaks can be observed which are related to crystallization reactions (named as the temperature of crystallization,  $T_x$ ) followed by the glassy transition. The large endothermic peak corresponds to the melting point ( $T_m$ ). The temperatures of  $T_g$ , first  $T_x$ , and  $T_m$ , as indicated by the arrows in Fig 1 (b), are 324.1, 349.8 and 717.2 K, respectively. The value of undercooling  $\Delta T = T_x - T_g$  and reduced glass transition temperature  $T_{rg} = T_g/T_m$  have been used as the important parameters [30–35] to identify the GFA. The values of  $\Delta T$  and  $T_{rg}$  for the amorphous  $\text{Ho}_{0.2}\text{Tm}_{0.2}\text{Gd}_{0.2}\text{Co}_{0.2}\text{Al}_{0.2}$  ribbon are 25.7 K and 0.5, respectively, which are better than most of the recently reported RE-based amorphous MC materials [33–37], illustrating the good GFA of the present studied amorphous  $\text{Ho}_{0.2}\text{Tm}_{0.2}\text{Gd}_{0.2}\text{Co}_{0.2}\text{Al}_{0.2}$  ribbon.

The temperature ( $T$ ) dependent magnetization ( $M$ ) herein was used to identify the magnetic phase transition (MPT) properties of the amorphous  $\text{Ho}_{0.2}\text{Tm}_{0.2}\text{Gd}_{0.2}\text{Co}_{0.2}\text{Al}_{0.2}$  ribbon. The field-cooling (FC) and zero-field-cooling (ZFC)  $M(T)$  curves (corresponding to left scale) of the amorphous  $\text{Ho}_{0.2}\text{Tm}_{0.2}\text{Gd}_{0.2}\text{Co}_{0.2}\text{Al}_{0.2}$  ribbon are given in Fig. 2(a) with magnetic field ( $H$ ) of 0.2 T. Significant signals from paramagnetic (PM) to ferromagnetic (FM) transition of the amorphous  $\text{Ho}_{0.2}\text{Tm}_{0.2}\text{Gd}_{0.2}\text{Co}_{0.2}\text{Al}_{0.2}$  ribbon can be noted. The MPT temperature

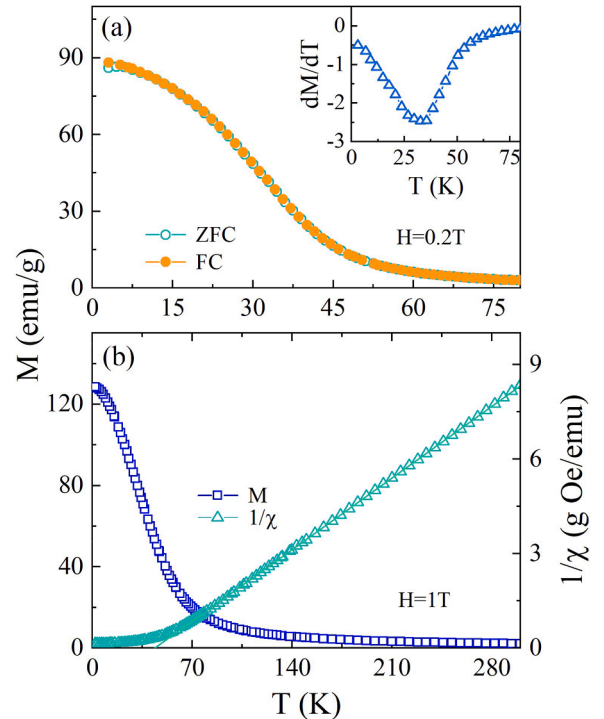


**Fig. 2.** (a)  $dM/dT$  ( $T$ ) and  $M(T)$  curves ( $H = 0.2$  T) of the amorphous  $\text{Ho}_{0.2}\text{Tm}_{0.2}\text{Gd}_{0.2}\text{Co}_{0.2}\text{Al}_{0.2}$  ribbon. (b)  $1/\chi(T)$  and  $M(T)$  curves ( $H = 1$  T) of the amorphous  $\text{Ho}_{0.2}\text{Tm}_{0.2}\text{Gd}_{0.2}\text{Co}_{0.2}\text{Al}_{0.2}$  ribbon.

( $T_C$ ) of the amorphous  $\text{Ho}_{0.2}\text{Tm}_{0.2}\text{Gd}_{0.2}\text{Co}_{0.2}\text{Al}_{0.2}$  ribbon is determined to be  $\sim 32.6$  K with the basis of the inflection point of temperature dependent  $dM/dT$  curves which were also given in Fig. 2(a) (corresponding to right scale). Moreover, only very tiny differences between the FC and ZFC curves at very low temperatures of the amorphous  $\text{Ho}_{0.2}\text{Tm}_{0.2}\text{Gd}_{0.2}\text{Co}_{0.2}\text{Al}_{0.2}$  ribbon can be noted, demonstrating no thermal hysteresis which is good for magnetic cooling. The  $M(T)$  curve (corresponding to left scale) together with the inverse susceptibility ( $1/\chi = H/M$ ; corresponding to right scale) of the amorphous  $\text{Ho}_{0.2}\text{Tm}_{0.2}\text{Gd}_{0.2}\text{Co}_{0.2}\text{Al}_{0.2}$  ribbon are given in Fig. 2(b) with  $H$  of 1 T. Notably, the  $1/\chi(T)$  curves in the PM region of the amorphous  $\text{Ho}_{0.2}\text{Tm}_{0.2}\text{Gd}_{0.2}\text{Co}_{0.2}\text{Al}_{0.2}$  ribbon obeying the Curie–Weiss law  $\chi(T) = C/(T - \theta_p)$ , where  $C$  and  $\theta_p$  represent the Curie constant and paramagnetic Curie temperature, respectively, and  $C = N(\mu_B\mu_{\text{eff}})^2/3k_B$  (where  $\mu_{\text{eff}}$  denotes the effective magnetic moment). The linear fittings above 120 K produced positive  $\theta_p$  value of 43.8 K of the amorphous  $\text{Ho}_{0.2}\text{Tm}_{0.2}\text{Gd}_{0.2}\text{Co}_{0.2}\text{Al}_{0.2}$  ribbon, which further confirms the FM ground state. The corresponding value of  $\mu_{\text{eff}}$  was determined to be  $8.91 \mu_B/f. u.$ , which is consistent well with the values by only considering the moment from rare earth ions ( $8.81 \mu_B/f. u.$ ). These results indicate that the rare earth ions play crucial roles in magnetism of the amorphous  $\text{Ho}_{0.2}\text{Tm}_{0.2}\text{Gd}_{0.2}\text{Co}_{0.2}\text{Al}_{0.2}$  ribbon.

To further explore the MPT and MC properties of the amorphous  $\text{Ho}_{0.2}\text{Tm}_{0.2}\text{Gd}_{0.2}\text{Co}_{0.2}\text{Al}_{0.2}$  ribbon, series magnetization isotherms, the  $M(H)$  curves, were measured which are given in Fig. 3(a). For the low temperature ones, the values of  $M$  increase abruptly with increasing  $H$  at low  $H$  region, and show saturation-like behavior at high  $H$  region, indicating FM state. For the ones with temperature above  $T_C$ , the values of  $M$  almost increase linearly with the increases of  $H$  in the scanning  $H$  regime, attributable to the PM state. Moreover, the MC effect and MC performances are strong related with the nature of corresponding MPT.

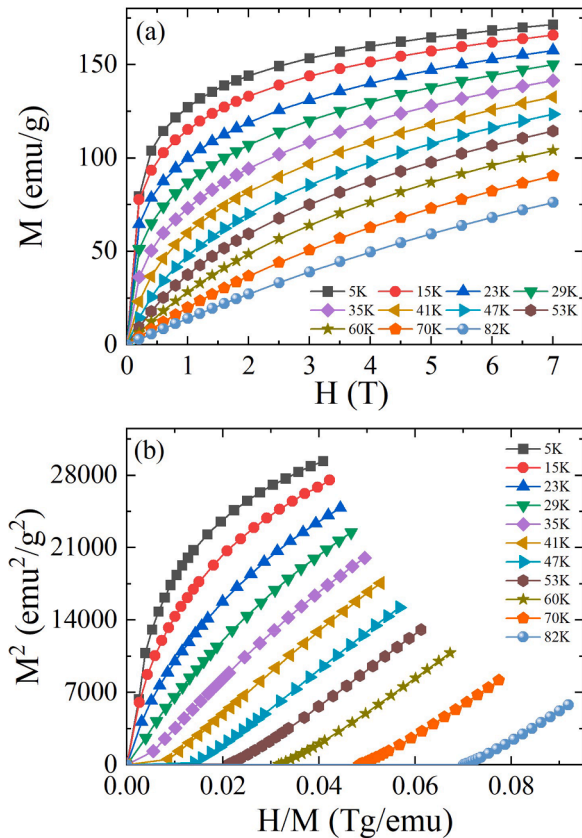


Fig. 3. (a)  $M(H)$  curves of the amorphous  $\text{Ho}_{0.2}\text{Tm}_{0.2}\text{Gd}_{0.2}\text{Co}_{0.2}\text{Al}_{0.2}$  ribbon. (b) Arrott-plots ( $H/M$  vs.  $M^2$ ) of the amorphous  $\text{Ho}_{0.2}\text{Tm}_{0.2}\text{Gd}_{0.2}\text{Co}_{0.2}\text{Al}_{0.2}$  ribbon.

Therefore, to examine its MPT order type of the amorphous  $\text{Ho}_{0.2}\text{Tm}_{0.2}\text{Gd}_{0.2}\text{Co}_{0.2}\text{Al}_{0.2}$  ribbon, the Arrott plot ( $H/M$  vs.  $M^2$ ) curves based on the Banerjee law [38] are given in Fig. 3(b) which were transferred directly based on the above given  $M(H)$  data. The positive and negative slopes in the Arrott plot curves [38] were the indicative of the second-order (SO-) and first-order (FO-) type MPT of the MC materials, respectively. The Arrott plot curves only exhibited positive slopes, demonstrating the SO-type MPT of the amorphous  $\text{Ho}_{0.2}\text{Tm}_{0.2}\text{Gd}_{0.2}\text{Co}_{0.2}\text{Al}_{0.2}$  ribbon.

Generally, the MC effect and MC performances can be identified primarily by the values of magnetic entropy change ( $\Delta S_M^{\text{max}}$ ) [2–4] which can be indirectly evaluated using the below equations:

$$\Delta S_M(T, \Delta H) = S_M(T, H) - S_M(T, 0) = \int_0^H \left( \frac{\partial S(H, T)}{\partial H} \right)_T dH. \quad (1)$$

Through Maxwell equation:

$$\left( \frac{\partial S(H, T)}{\partial H} \right)_T = \left( \frac{\partial M(H, T)}{\partial T} \right)_H, \quad (2)$$

then,

$$\Delta S_M(T, \Delta H) = S_M(T, H) - S_M(T, 0) = \int_0^H \left( \frac{\partial M(H, T)}{\partial T} \right)_H dH. \quad (3)$$

The calculated temperature dependent  $-\Delta S_M$  curves of the amorphous  $\text{Ho}_{0.2}\text{Tm}_{0.2}\text{Gd}_{0.2}\text{Co}_{0.2}\text{Al}_{0.2}$  ribbon are given in Fig. 4(a). Only positive  $-\Delta S_M$  values can be observed in the overall measuring temperature zone and exhibit a broad pronounced peak around  $T_C$  ( $\sim 32.6$  K), i. e., a nearly table-like shape can be noted which is desirable for practical MR applications. The maximum  $-\Delta S_M$  values ( $-\Delta S_M^{\text{max}}$ ) increase gradually with increasing  $\Delta H$ . Under  $\Delta H$  of 0–1, 0–3, 0–5 T, and 0–7 T, the  $-\Delta S_M$  values of the amorphous  $\text{Ho}_{0.2}\text{Tm}_{0.2}\text{Gd}_{0.2}\text{Co}_{0.2}\text{Al}_{0.2}$  ribbon are found to be 2.2, 6.3, 9.9, and 13.0 J/kgK, respectively. Additionally, a phenomenological  $-\Delta S_M(T)$  universal curve [39] of the MC materials with SO-type MPT was proposed by changing the  $Y$  and  $X$  axes to  $\Delta S_T(T)/\Delta S_M^{\text{max}}$  and  $\theta$ , respectively. The  $\theta$  is expressed above and below  $T_C$  independently, as follows:

$$\theta = \begin{cases} -(T - T_C)/(T_{r1} - T_C) & \text{for } T \leq T_C \\ (T - T_C)/(T_{r2} - T_C) & \text{for } T > T_C \end{cases} \quad (5)$$

Here,  $T_{r1}$  and  $T_{r2}$  ( $T_{r1} < T_C < T_{r2}$ ), corresponding to  $\Delta S(T_{r1}, T_{r2}) = 0.6 \times \Delta S_M^{\text{max}}$ , are two reference temperatures. The constructed  $\Delta S_M/\Delta S_M^{\text{max}}$  vs.  $\theta$  curves of the amorphous  $\text{Ho}_{0.2}\text{Tm}_{0.2}\text{Gd}_{0.2}\text{Co}_{0.2}\text{Al}_{0.2}$  ribbon are given in Fig. 4(b). All the curves are well collapse into a single line, further confirming the SO-type MPT of the amorphous  $\text{Ho}_{0.2}\text{Tm}_{0.2}\text{Gd}_{0.2}\text{Co}_{0.2}\text{Al}_{0.2}$  ribbon.

In addition to  $-\Delta S_M$ , the parameters of temperature-averaged entropy changes ( $TEC$ , as given in Eq. (6)) [40] and refrigerant capacity ( $RC$ , as given in Eq. (7)) [2–4] were also well used to identify the performance of MC materials based on experimentally obtained  $-\Delta S_M(T)$  results.

$$TEC(\Delta T_{\text{lift}}) = \frac{1}{\Delta T_{\text{lift}}} \max_{T_{\text{mid}}} \left\{ \int_{T_{\text{mid}} - \frac{\Delta T_{\text{lift}}}{2}}^{T_{\text{mid}} + \frac{\Delta T_{\text{lift}}}{2}} \Delta S_M(T) \Delta H, T dT \right\}, \quad (6)$$

$$RC = \int_{T_{\text{cold}}}^{T_{\text{hot}}} |\Delta S_M(T)| dT \quad (7)$$

In which, the  $T_{\text{mid}}$  represents the central temperature where  $TEC$  ( $\Delta T_{\text{lift}}$ ) reaches the maximum value. The  $T_{\text{cold}}$  and  $T_{\text{hot}}$  represent the temperatures with  $\frac{1}{2} |\Delta S_M^{\text{max}}|$  values at both sides in the  $\Delta S_M(T)$  curves. Here, the  $\Delta T_{\text{lift}}$  of 10 and 20 K were selected, and the resulted  $TEC(10)/TEC(20)$  values of the amorphous  $\text{Ho}_{0.2}\text{Tm}_{0.2}\text{Gd}_{0.2}\text{Co}_{0.2}\text{Al}_{0.2}$  ribbon under  $\Delta H$  of 0–3 and 0–7 T were obtained to be 8.2/8.0 and 13.0/12.7 J/kgK, respectively. The corresponding  $RC$  values were obtained to be 265.5 and 341.4 J/kg, respectively. For more details, the  $\Delta H$

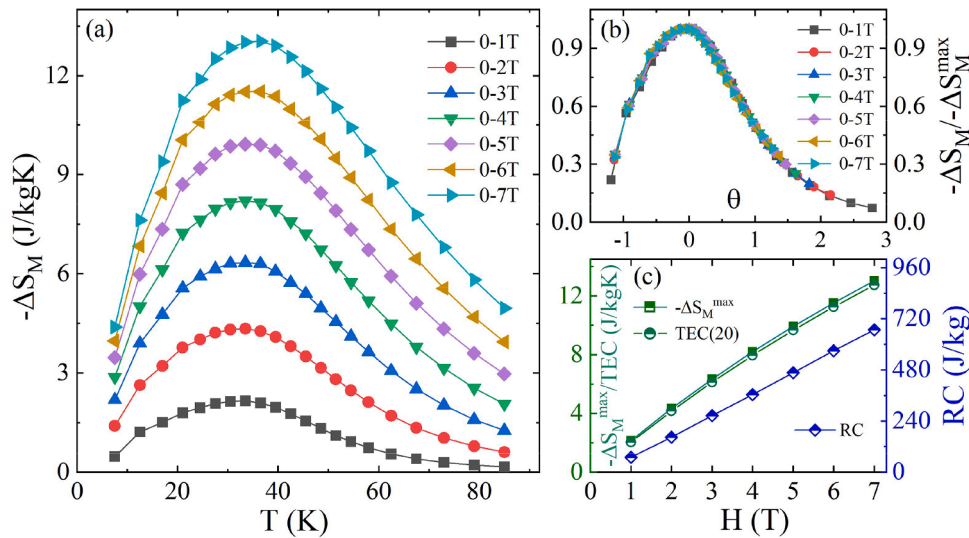


**Fig. 4.** (a)  $-\Delta S_M$  curves of the amorphous  $\text{Ho}_{0.2}\text{Tm}_{0.2}\text{Gd}_{0.2}\text{Co}_{0.2}\text{Al}_{0.2}$  ribbon. (b) Constructed  $\Delta S_M / \Delta S_M^{max}$  versus  $\theta$  curves of the amorphous  $\text{Ho}_{0.2}\text{Tm}_{0.2}\text{Gd}_{0.2}\text{Co}_{0.2}\text{Al}_{0.2}$  ribbon. (c)  $\Delta H$  dependence of  $-\Delta S_M^{max}$  and  $TEC(20)$ , and  $RC$  of the amorphous  $\text{Ho}_{0.2}\text{Tm}_{0.2}\text{Gd}_{0.2}\text{Co}_{0.2}\text{Al}_{0.2}$  ribbon

dependence of  $-\Delta S_M^{max}$  and  $TEC(20)$  (corresponding to left scale) together with  $RC$  (corresponding to right scale) of the amorphous  $\text{Ho}_{0.2}\text{Tm}_{0.2}\text{Gd}_{0.2}\text{Co}_{0.2}\text{Al}_{0.2}$  ribbon are given in Fig. 4(c), respectively. All these MC parameters show similar tendency, i.e., an increased  $\Delta H$  results in the increase of the MC parameters of the amorphous  $\text{Ho}_{0.2}\text{Tm}_{0.2}\text{Gd}_{0.2}\text{Co}_{0.2}\text{Al}_{0.2}$  ribbon. Moreover, the above-mentioned MC parameters of  $-\Delta S_M^{max}$ ,  $TEC(10)$ , and  $RC$  under  $\Delta H$  of 0–5 T of the amorphous  $\text{Ho}_{0.2}\text{Tm}_{0.2}\text{Gd}_{0.2}\text{Co}_{0.2}\text{Al}_{0.2}$  ribbon are at similarly high level with some of recently updated low temperature  $RE$ -based MC materials, such as, amorphous  $\text{RE}_{55}\text{Co}_{30}\text{Al}_{10}\text{Si}_5$  ribbons [34],  $\text{La}_{1-x}\text{Pr}_x\text{Fe}_{12}\text{B}_6$  compounds [41], amorphous  $\text{Fe}_{35}\text{RE}_{65}$  alloys [42],  $\text{RE}_3\text{RuO}_7$  oxides [43], amorphous  $\text{RE}_{55}\text{Ni}_{18}\text{Al}_{27}$  ribbons [36],  $\text{RENiGa}_2$  compounds [44], amorphous  $\text{Cu}_{18}\text{Al}_{25}\text{RE}_{57}$  alloys [45],  $\text{RE}_2\text{Cr}_2\text{C}_3$  compounds [46] etc., making the present amorphous  $\text{Ho}_{0.2}\text{Tm}_{0.2}\text{Gd}_{0.2}\text{Co}_{0.2}\text{Al}_{0.2}$  ribbon also attractive for low temperature magnetic cooling.

#### 4. Conclusions

In summary, the amorphous  $\text{Ho}_{0.2}\text{Tm}_{0.2}\text{Gd}_{0.2}\text{Co}_{0.2}\text{Al}_{0.2}$  ribbon was fabricated by melt-spun method and systematically investigated its structure, GFA, MPT, MC effect and MC performance. The melt-spun  $\text{Ho}_{0.2}\text{Tm}_{0.2}\text{Gd}_{0.2}\text{Co}_{0.2}\text{Al}_{0.2}$  alloy shows a fully amorphous structure nature and good GFA. The amorphous  $\text{Ho}_{0.2}\text{Tm}_{0.2}\text{Gd}_{0.2}\text{Co}_{0.2}\text{Al}_{0.2}$  ribbon undergoes a second order type MPT around 32.6 K from FM to PM state. Large reversible low temperature MC effect and good MC performances in the amorphous  $\text{Ho}_{0.2}\text{Tm}_{0.2}\text{Gd}_{0.2}\text{Co}_{0.2}\text{Al}_{0.2}$  ribbon were realized. The obtained  $-\Delta S_M^{max}$ ,  $TEC(10)$  and  $RC$  values for the amorphous  $\text{Ho}_{0.2}\text{Tm}_{0.2}\text{Gd}_{0.2}\text{Co}_{0.2}\text{Al}_{0.2}$  ribbon under  $\Delta H$  of 0–7 T are 13.0 J/kgK, 13.0 J/kgK, and 668.4 J/kg, respectively. These findings indicating that the amorphous  $\text{Ho}_{0.2}\text{Tm}_{0.2}\text{Gd}_{0.2}\text{Co}_{0.2}\text{Al}_{0.2}$  ribbon could be a good candidate for magnetic cooling at low temperatures.

#### CRediT authorship contribution statement

**Yongyun Shu:** Data curation, Investigation, Validation, Writing – original draft. **Longfei Wang:** Data curation, Investigation, Methodology, Validation. **Silu Huang:** Formal analysis, Investigation, Methodology. **Yikun Zhang:** Conceptualization, Project administration, Supervision, Writing – original draft, Writing – review & editing.

#### Declaration of competing interest

The authors declare that they have no known competing financial interests or personal relationships that could have appeared to influence the work reported in this paper.

#### Data availability

Data will be made available on request.

#### Acknowledgments

The present work was supported by the “Pioneer” and “Leading Goose” R&D Program of Zhejiang (Grant No. 2022C01230).

#### References

- [1] O. Gutfleisch, M.A. Willard, E. Brück, C.H. Chen, S.G. Sankar, J.P. Liu, Magnetic materials and devices for the 21st century: Stronger, lighter, and more energy efficient, *Adv. Mater.* 23 (2011) 821.
- [2] V. Franco, J. Blázquez, J. Iplus, J. Law, L. Ramfréze, A. Comde, Magnetocaloric effect: From materials research to refrigeration devices, *Prog. Mater. Sci.* 93 (2018) 112.
- [3] L.W. Li, M. Yan, Recent progress in the development of  $\text{RE}_2\text{TMTM}'\text{O}_6$  double perovskite oxides for cryogenic magnetic refrigeration, *J. Mater. Sci. Technol.* 136 (2023) 1.
- [4] L.W. Li, M. Yan, Recent progresses in exploring the rare earth based intermetallic compounds for cryogenic magnetic refrigeration, *J. Alloy. Compd.* 823 (2020) 153810.
- [5] J.C. Lin, P. Tong, X.K. Zhang, Z.C. Wang, Z. Zhang, B. Li, G.H. Zhong, J. Chen, Y. D. Wu, H.L. Lu, L.H. He, B. Bai, L.S. Lin, W.H. Song, Z.D. Zhang, Y.P. Sun, Giant room-temperature barocaloric effect at the electronic phase transition in  $\text{Ni}_{1-x}\text{Fe}_x\text{S}$ , *Mater. Horiz.* 7 (2020) 2690.
- [6] T. Gottschall, A. Gràcia-Condal, M. Fries, A. Taubel, L. Pfeuffer, L. Mañosa, A. Planes, K.P. Skokov, O. Gutfleisch, A multicaloric cooling cycle that exploits thermal hysteresis, *Nat. Mater.* 17 (2018) 929.
- [7] J.C. Lin, P. Tong, K. Zhang, W. Lu, X. Wang, X. Zhang, W. Song, Y.P. Sun, Colossal and reversible barocaloric effect in liquid-solid-transition materials n-alkanes, *Nat. Commun.* 12 (2022) 596.
- [8] Y. Wang, L. Wang, J. Xia, Z. Lai, G. Tian, X. Zhang, Z. Hou, X. Gao, W. Mi, M. Zeng, G. Zhou, G. Yu, G. Wu, Y. Zhou, W. Wang, X.X. Zhang, J.M. Liu, Electric-field-driven non-volatile multi-state switching of individual skyrmions in a multiferroic heterostructure, *Nat. Commun.* 11 (2020) 3577.
- [9] J.Y. Law, V. Franco, Pushing the limits of magnetocaloric high-entropy alloys, *APL Mater.* 9 (2021) 080702.
- [10] Z. Guan, J. Bai, Y. Zhang, J. Gu, N. Morley, C. Esling, Y. Zhang, X. Zhao, L. Zuo, Ni-Co-Mn-Ti-B high performance multiferroic phase transformation material: Simultaneous modulation of mechanical properties and successive caloric effects by B doping, *Mater. Today Phys.* 36 (2023) 101183.

- [11] Y.K. Zhang, W.X. Hao, C.L. Hu, X. Wang, X.F. Zhang, L.W. Li, Rare-Earth-Free  $\text{Mn}_{30}\text{Fe}_{20-x}\text{Cu}_x\text{Al}_{50}$  Magnetocaloric Materials with Stable Cubic CsCl-type Structure for Room-Temperature Refrigeration, *Adv. Funct. Mater.* 33 (2023) 2310047.
- [12] Y.K. Zhang, P. Xu, J. Zhu, S.M. Yan, J.C. Zhang, L.W. Li, The emergence of considerable room temperature magnetocaloric performances in the transition metal high-entropy alloys, *Mater. Today Phys.* 32 (2023) 101031.
- [13] L. Miao, X. Lu, Z. Wei, Y. Zhang, J. Liu, Enhanced mechanical strength in hot-rolled La-Fe-Si/Fe magnetocaloric composites by microstructure manipulation, *Acta Mater.* 245 (2023) 118635.
- [14] L. Li, P. Xu, S. Ye, Y. Li, G. Liu, D. Huo, M. Yan, Magnetic properties and excellent cryogenic magnetocaloric performances in B-site ordered  $\text{RE}_2\text{ZnMnO}_6$  ( $\text{RE} = \text{Gd}$ , Dy and Ho) perovskites, *Acta Mater.* 194 (2020) 354.
- [15] L. Li, C. Xu, Y. Yuan, S. Zhou, Achievement of a table-like magnetocaloric effect in the dual-phase  $\text{ErZn}_2/\text{ErZn}$  composite, *Mater. Res. Lett.* 6 (2018) 67.
- [16] L. Li, O. Niehaus, M. Kersting, R. Pöttgen, Reversible table-like magnetocaloric effect in  $\text{Eu}_4\text{PdMg}$  over a very large temperature span, *Appl. Phys. Lett.* 104 (2014) 092416.
- [17] W. Liu, E. Bykov, S. Taskaev, M. Bogush, V. Khovaylo, N. Fortunato, A. Aubert, H. Zhang, T. Gottschall, J. Wosnitza, F. Scheibel, K. Skokov, O. Gutfleisch, A study on rare-earth Laves phases for magnetocaloric liquefaction of hydrogen, *Appl. Mater. Today* 29 (2022) 101624.
- [18] Y.K. Zhang, J.Y. Ying, X.Q. Gao, Z.J. Mo, J. Shen, L.W. Li, Exploration of the rare-earth cobalt nickel-based magnetocaloric materials for hydrogen liquefaction, *J. Mater. Sci. Technol.* 159 (2023) 163.
- [19] Y. Zhang, J. Zhu, S. Li, J. Wang, Z. Ren, Achievement of giant cryogenic refrigerant capacity in quinary rare-earths based high-entropy amorphous alloy, *J. Mater. Sci. Technol.* 102 (2022) 66.
- [20] Z. Ma, P. Xu, J. Ying, Y. Zhang, L. Li, Insight into the structural and magnetic properties of  $\text{RECo}_{12}\text{B}_6$  ( $\text{RE} = \text{Ce}$ , Pr, Nd) compounds: A combined experimental and theoretical investigation, *Acta Mater.* 247 (2023) 118757.
- [21] Y.K. Zhang, Y. Tian, Z. Zhang, Y. Jia, S. Li, B. Zhang, J. Wang, Z. Ren, Magnetic properties and giant cryogenic magnetocaloric effect in B-site ordered antiferromagnetic  $\text{Gd}_2\text{MgTiO}_6$  double perovskite oxide, *Acta Mater.* 226 (2022) 117669.
- [22] Y.K. Zhang, J. Zhu, S. Li, Z.Q. Zhang, J. Wang, Z.M. Ren, Magnetic properties and promising cryogenic magnetocaloric performances in the antiferromagnetic  $\text{GdFe}_2\text{Si}_2$  compound, *Sci. China Mater.* 65 (2022) 1345.
- [23] X. Wang, L. Wang, N.L. Gulay, L. Li, R. Pottgen, Magnetic phase transition and magnetocaloric effect of  $\text{RE}_2\text{RuIn}$  ( $\text{RE} = \text{Dy}$ , Ho, ErTm), *J. Magn. Magn. Mater.* 589 (2024) 171406.
- [24] B. Wu, Y. Zhang, D. Guo, J. Wang, Z. Ren, Structure, magnetic properties and cryogenic magneto-caloric effect (MCE) in  $\text{RE}_2\text{FeAlO}_6$  ( $\text{RE} = \text{Gd}$ , Dy, Ho) oxides, *Ceram. Int.* 46 (2021) 6290.
- [25] S.X. Yang, X.Q. Zheng, D. Wang, J. Xu, W. Yin, L. Xi, C. Liu, J. Liu, J. Xu, H. Zhang, Z. Xu, L. Wang, Y. Yao, M. Zhang, Y. Zhang, J. Shen, S.G. Wang, B.G. Shen, Giant low-field magnetocaloric effect in ferromagnetically ordered  $\text{Er}_{1-x}\text{Tm}_x\text{Al}_2$  ( $0 \leq x \leq 1$ ) compounds, *J. Mater. Sci. Technol.* 146 (2023) 168.
- [26] Y. Zhang, W. Hao, J. Shen, Z. Mo, T. Gottschall, L. Li, Investigation of the structural and magnetic properties in the  $\text{GdCoC}$  compound featuring excellent cryogenic magnetocaloric performances, *Acta Mater.* (2024).
- [27] J.J. Gong, Z.J. Mo, Y.P. Wang, Z.X. Li, L. Zhang, Q. Fu, Y. Li, J. Shen, Superexchange antiferromagnetism and cryogenic magnetocaloric effect in scheelite-type  $\text{GdT}_{0.5}\text{Mo}_{0.5}\text{O}_4$  compound, *Ceram. Int.* 51 (2024) 950.
- [28] Z.J. Mo, J. Gong, H. Xie, L. Zhang, Q. Fu, X.Q. Gao, Z. Li, J. Shen, Giant and reversible low field magnetocaloric effect in  $\text{LiHoF}_4$  compound, *Chin. Phys. B* 32 (2023) 027503.
- [29] P. Xu, L. Hu, Z. Zhang, H. Wang, L.W. Li, Electronic structure, magnetic properties and magnetocaloric performance in rare earths (RE) based  $\text{RE}_2\text{BaZnO}_5$  ( $\text{RE} = \text{Gd}$ , Dy, Ho, and Er) compounds, *Acta Mater.* 236 (2022) 118114.
- [30] L.L. Pan, Q. Wang, X. Zhou, B.Z. Tang, P. Yu, D. Ding, L. Xi, Glass formability of the Tb-Ni binary alloys and the magnetic properties of the Tb<sub>65</sub>Ni<sub>35</sub> metallic glass, *Intermetallics* 148 (2022) 107650.
- [31] M. Lassri, S. El Ouahbi, M. Sajjeddine, A. Berrada, N. Hassanain, Investigation of the Correlation Between the Critical Behavior and the Magnetocaloric Effect of Amorphous  $\text{Eu}_{80}\text{Au}_{20}$  Alloy, *J. Electron. Mater.* 52 (2023) 6080.
- [32] F. Jin, C.M. Pang, X.M. Wang, C.C. Yuan, The role of rare earth elements in tailorable thermal and magnetocaloric properties of RE-Co-Al ( $\text{RE} = \text{Gd}$ , Tb, and Dy) metallic glasses, *J. Non Cryst. Solids* 600 (2023) 121992.
- [33] Y. Ma, H. Yin, F. Chen, M. Gao, L. Song, Y. Zhang, W. Xu, L.M. Wang, J.T. Huo, S. Z. Zhang, J.Q. Wang, Magnetocaloric effect in (Tm<sub>67</sub>Cu<sub>33</sub>)<sub>80</sub>Al<sub>20</sub> amorphous alloy, *J. Non Cryst. Solids* 604 (2023) 122151.
- [34] L. Tian, Q. Fu, Z.J. Mo, H. Sun, Z.X. Li, J. Shen, G.D. Liu, Magnetic and magnetocaloric properties of  $\text{R}_{55}\text{Co}_{30}\text{Al}_{10}\text{Si}_5$  ( $\text{R} = \text{Ho}$ , Dy) metallic glass ribbons, *J. Magn. Magn. Mater.* 576 (2023) 17077.
- [35] L. Lindner, Z. Śniadecki, M. Kołodziej, J.M. Grenèche, J. Marcin, I. Škorvánek, B. Idzikowski, Tunable magnetocaloric effect in amorphous Gd-Fe-Co-Al-Si alloys, *J. Mater. Sci.* 57 (2022) 553.
- [36] Y. Jia, X. Zhao, X. Liu, L. Li, Magnetic properties and magnetocaloric performances in amorphous  $\text{RE}_{55}\text{Ni}_{18}\text{Al}_{27}$  ( $\text{RE} = \text{Ho}$ , Er and Tm) ribbons, *J. Alloy. Compd.* 813 (2020) 152177.
- [37] L. Xue, L. Shao, Z. Han, Q. Luo, H. Wang, J. Huo, Z. Li, B. Zhang, J. Cheng, B. Shen, Tunable magnetocaloric effect in Gd-based metallic glasses microalloying elements with different magnetism, *J. Non Cryst. Solids* 576 (2022) 121222.
- [38] B.K. Banerjee, On a generalised approach to first and second order magnetic transitions, *Phys. Lett.* 12 (1964) 16–17.
- [39] V. Franco, A. Conde, Scaling laws for the magnetocaloric effect in second order phase transitions: from physics to applications for the characterization of materials, *Int. J. Refrig.* 33 (2010) 465.
- [40] L.D. Griffith, Y. Mudryk, J. Slaughter, V.K. Pecharsky, Material-based figure of merit for caloric materials, *J. Appl. Phys.* 123 (2018) 034902.
- [41] Z.P. Ma, X.S. Dong, Z.Q. Zhang, L.W. Li, Achievement of promising cryogenic magnetocaloric performances in  $\text{La}_{1-x}\text{Pr}_x\text{Fe}_{12}\text{B}_6$  compounds, *J. Mater. Sci. Technol.* 92 (2021) 138.
- [42] A. Elouafi, S. Ezairi, F. Lmai, A. Tizliouine, Excellent magnetocaloric effect at cryogenic temperature in amorphous ( $\text{Fe}_{35}\text{RE}_{65}$ ) ( $\text{RE} = \text{Er}$ , Dy and Gd) alloys, *J. Magn. Magn. Mater.* 588 (2023) 171381.
- [43] N. He, P. Wang, J. Huang, X. Wang, Y. Zhang, L. Hu, L. Li, M. Yan, Structural, magnetic and magnetocaloric properties in the rare earth ruthenate  $\text{RE}_3\text{RuO}_7$  ( $\text{RE} = \text{Pr}$ , Nd, Gd and Tb) oxides with fluorite related structure, *Ceram. Int.* 48 (2022) 36968.
- [44] D. Guo, L.M.M. Ramírez, J.Y. Law, Y.K. Zhang, V. Franco, Excellent cryogenic magnetocaloric properties in heavy rare-earth based  $\text{HRENiGa}_2$  ( $\text{HRE} = \text{Dy}$ , Ho or Er) compounds, *Sci. China Mater.* 66 (2023) 249.
- [45] Z. Dong, S. Yin, Structural, magnetic and magnetocaloric performances in  $\text{Cu}_{18}\text{Al}_{25}\text{Ho}_{57}$  and  $\text{Cu}_{18}\text{Al}_{25}\text{Tm}_{57}$  amorphous ribbons, *J. Magn. Magn. Mater.* 495 (2020) 165888.
- [46] Y.K. Zhang, S. Li, L. Hu, X.H. Wang, L. Li, M. Yan, Excellent magnetocaloric performance in the carbide compounds  $\text{RE}_2\text{Cr}_2\text{C}_3$  ( $\text{RE} = \text{Er}$ , Ho, and Dy) and their composites, *Mater. Today Phys.* 27 (2022) 100786.